Applied Numerical Mathematics 156 (2020) 608–626

Contents lists available at ScienceDirect

Applied Numerical Mathematics

www.elsevier.com/locate/apnum

Well-balanced central schemes for the one and two-dimensional Euler systems with gravity

F. Kanbar [a,b], R. Touma [b,*], C. Klingenberg [a]

[a] Mathematics, University of Wuezburg, Germany
[b] Mathematics, Lebanese American University, Lebanon

ARTICLE INFO

Article history:
Received 18 June 2019
Received in revised form 17 April 2020
Accepted 15 May 2020
Available online 1 June 2020

Keywords:
Euler equations
Unstaggered central schemes
Well-balanced schemes
Stationary solutions

ABSTRACT

In this paper we develop a family of central schemes for the one and two-dimensional systems of Euler equations with gravitational source term. The proposed schemes are unstaggered, second-order, central finite volume schemes that avoid solving Riemann problems at the cell interfaces and avoid switching between an original and a staggered grid. The main feature of the schemes developed here is that they are capable of preserving any steady state of the Euler with gravity system up to machine accuracy by updating the numerical solution in terms of a relevant reference solution. The methodology proposed results in a well-balanced scheme capable of capturing any steady state. Our scheme is then implemented and used to solve classical problems from the recent literature.

1. Introduction

Euler equations with gravitational source term are widely studied because of their importance in modeling physical phenomena such as astrophysical and atmospheric phenomena including supernova explosions [16], climate modeling, and weather forecasting [5]. The two-dimensional Euler system with gravity is given by:

$$\begin{cases} \mathbf{U}_t + F(\mathbf{U})_x + G(\mathbf{U})_y = S(\mathbf{U}), & (x, y) \in \Omega \subset \mathbb{R}^2,\ t > 0 \\ \mathbf{U}(x, y, 0) = \mathbf{U}_0(x, y) \end{cases} \tag{1}$$

where

$$\mathbf{U} = \begin{pmatrix} \rho \\ \rho u \\ \rho v \\ E \end{pmatrix} F(\mathbf{U}) = \begin{pmatrix} \rho u \\ \rho u^2 + p \\ \rho uv \\ (E + p)u \end{pmatrix} G(\mathbf{U}) = \begin{pmatrix} \rho v \\ \rho uv \\ \rho v^2 + p \\ (E + p)v \end{pmatrix}$$

$$S(\mathbf{U}) = \begin{pmatrix} 0 \\ -\rho\phi_x \\ -\rho\phi_y \\ -\rho u\phi_x - \rho v\phi_y \end{pmatrix}$$

* Corresponding author.
E-mail address: rony.touma@lau.edu.lb (R. Touma).

https://doi.org/10.1016/j.apnum.2020.05.010
0168-9274/

ρ is the fluid density, u and v are velocity components in the x and y-directions, respectively. The pressure is p and the non-gravitational energy is $E = \frac{1}{2}\rho(u^2+v^2) + \frac{p}{\gamma-1}$ includes the kinetic and internal energy of the fluid. The gravitational potential $\phi = \phi(x,y)$ is a given function and γ is the ratio of specific heats. Of particular interest are stationary solutions with zero velocity called hydrostatic equilibrium. In order to properly capturing these steady states one should apply a well-balanced numerical scheme especially designed for the Euler with gravity systems. Several attempts were previously made for computation of the numerical solution of system (1) and some of them are listed here [4,6,7,9,10,18,25–30]. One way to fulfill the well-balanced requirement of the numerical scheme is by designing the discretization in the source term in the balance law by following that of the divergence of the flux function. In this work we follow a special reconstruction in the conservative variables that will fulfill the well-balanced requirement and will allow a proper capture of the steady states. This well-balanced approach will be blended with the unstaggered central finite volume scheme for hyperbolic systems of conservation laws [19]. The main reason behind choosing central schemes as base scheme relies in the fact that central schemes are easy to implement and robust finite volume schemes that avoid the time consuming process of solving Riemann problems arising at the cell interfaces. Furthermore central schemes have proved to be efficient schemes for the simulation of systems of hyperbolic conservation laws. Nessyahu and Tadmor (NT) have introduced in [17] a non-oscillatory central finite volume scheme that is based on evolving piecewise linear numerical solution on two staggered grids. Useful extensions of the NT scheme to multi space dimensions followed in [1–3,11,13,14,22]. These extensions were successfully used to problems arising in aerodynamics, hydrodynamics, and magnetohydrodynamics [3,8,20,21].

In order to avoid switching between an original and a staggered grid in the NT-type schemes, unstaggered central schemes (UCS) for hyperbolic systems of conservation laws were developed in [15,19], where the numerical solution is evolved on a single grid. The UCS schemes were then extended to the case of hyperbolic balance laws such as shallow water equations on variable waterbeds, Ripa systems, and Euler with gravity systems [20,23–25]. The main idea of the UCS schemes is to evolve the numerical solution on a single grid and to use a staggered ghost grid in an intermediate step, followed by a back projection step. In [25], a central well-balanced, unstaggered, and second-order accurate scheme for Euler system with gravity has been developed. As is in most of well-balanced schemes for Euler with gravity systems, the scheme is designed in a particular way so that it can preserve the hydrostatic equilibrium. The way to achieve this is by following a special discretization of the gravitational source term and forcing it to follow the discretization of the divergence of the flux term. This was completed by using sensor functions on the limiter that approximates these spatial derivatives. This particular reformulation of the source term was pretty efficient in preserving the hydrostatic equilibrium and in solving other Euler's problems. However, the numerical scheme presented in [25] can only preserve one type of steady states, mainly steady states with a zero velocity field. In this paper we develop a family of well-balanced, unstaggered, second-order accurate, central schemes for the Euler system with gravity that is capable of capturing any steady state of the system. The proposed method follows the reconstruction method developed in [4]; it consists of evolving the error function between the vector of conserved variables and a given steady state, instead of evolving the vector of conserved variables. This error function is defined as $\Delta\mathbf{U} = \mathbf{U} - \tilde{\mathbf{U}}$, where $\tilde{\mathbf{U}}$ is a given steady state. Knowing the steady state (analytically or numerically) is a key ingredient for the implementation of the proposed scheme. The detailed presentation of the proposed method is given in sections 2 and 3. In subsection 2.3, we prove that a scalar version of the UCS is TVD. The proposed scheme is implemented in section 4 and classical test case problems are considered both in one and two space dimensions. Concluding remarks and future work ideas are given in section 5.

2. Unstaggered well-balanced central scheme for the one-dimensional Euler system with gravity

In this section we develop a new well-balanced central scheme for the one-dimensional Euler system with gravitational source term. The proposed method follows the reconstruction method previously presented in [4].

2.1. One-dimensional Euler system with gravity

The one-dimensional Euler system with gravity is given by

$$\begin{cases} \mathbf{u}_t + f(\mathbf{u})_x = S(\mathbf{u}), \qquad x \in \Omega \subset \mathbb{R},\ t > 0 \\ \mathbf{u}(x,0) = \mathbf{u}_0(x) \end{cases} \tag{2}$$

where

$$\mathbf{u} = \begin{pmatrix} \rho \\ \rho u \\ E \end{pmatrix} f(\mathbf{u}) = \begin{pmatrix} \rho u \\ \rho u^2 + p \\ (E+p)u \end{pmatrix} S(\mathbf{u}) = \begin{pmatrix} 0 \\ -\rho\phi_x \\ -\rho u \phi_x \end{pmatrix}$$

Here ρ is the fluid density, u is the velocity, p is the pressure and $E = \frac{1}{2}\rho u^2 + \frac{p}{\gamma-1}$ is the non-gravitational energy which includes the kinetic and internal energy of the fluid. The gravitational potential $\phi = \phi(x)$ is a given function and γ is the ratio of specific heats. In the absence of gravity, system (2) reduces to a hyperbolic system of conservation laws with a complete set of real eigenvalues and a corresponding set of linearly independent eigenvectors.

2.2. The one-dimensional unstaggered FV central scheme

We consider for our computational domain Ω an interval of the real axis, and we partition it using the control cells defined to be the subintervals $C_i = \left[x_{i-\frac{1}{2}}, x_{i+\frac{1}{2}}\right]$ of equal width $\Delta x = x_{i+\frac{1}{2}} - x_{i-\frac{1}{2}}$ and centered at the nodes x_i. We also define the dual ghost cells $D_{i+\frac{1}{2}} = [x_i, x_{i+1}]$ with centers $x_{i+\frac{1}{2}} = x_i + \frac{\Delta x}{2}$. The time step will be denoted by Δt, and for a positive integer n we set $t^{n+1} = t^n + \Delta t$.

We assume that the numerical solution $\mathbf{u}_i^n$ at time t^n is known at the nodes x_i where $\mathbf{u}_i^n$ is used to approximate the exact solution $\mathbf{u}(x_i, t^n)$. The numerical base scheme evolves a piecewise linear solution $\mathcal{L}_i(x,t)$ that approximates the analytic solution $\mathbf{u}(x,t)$ with

$$\mathbf{u}_i^n = \frac{1}{\Delta x}\int_{C_i} \mathcal{L}_i(x,t)\,dx \approx \frac{1}{\Delta x}\int_{C_i} \mathbf{U}_i(x,t)\,dx.$$

Before proceeding with the presentation of the numerical scheme we introduce some notations that will be used throughout the remaining of the paper. In order to approximate the spatial numerical derivatives, the (MC-θ) limiter is considered which is defined as

$$(\mathbf{u}_i^n)' = \text{minmod}\left[\theta\frac{\mathbf{u}_i^n - \mathbf{u}_{i-1}^n}{\Delta x}, \frac{\mathbf{u}_{i+1}^n - \mathbf{u}_{i-1}^n}{2\Delta x}, \theta\frac{\mathbf{u}_{i+1}^n - \mathbf{u}_i^n}{\Delta x}\right]$$

where θ is a parameter that takes any value $1 < \theta < 2$, while the minmod function is defined as:

$$\text{minmod}(a,b,c) = \begin{cases} \text{sign}(a)\min\{|a|,|b|,|c|\}, & \text{if } \text{sign}(a) = \text{sign}(b) = \text{sign}(c) \\ 0, & \text{Otherwise.} \end{cases}$$

We start the derivation of our numerical scheme by first assuming that $\tilde{\mathbf{u}}$ is a given stationary solution of system (2), and we follow the reconstruction approach previously presented in [4] as follows. Let $\Delta\mathbf{u} = \mathbf{u} - \tilde{\mathbf{u}}$, we substitute $\mathbf{u} = \Delta\mathbf{u} + \tilde{\mathbf{u}}$ in the balance law in system (2):

$$\mathbf{u}_t + f(\mathbf{u})_x = S(\mathbf{u}), \tag{3}$$

and taking into account that $\tilde{\mathbf{u}}$ is a stationary solution, this results in:

$$\Delta\mathbf{u}_t + f(\Delta\mathbf{u} + \tilde{\mathbf{u}})_x = S(\Delta\mathbf{u} + \tilde{\mathbf{u}}). \tag{4}$$

On the other hand, since $\tilde{\mathbf{u}}$ is a stationary solution of (3), then the balance law reduces to:

$$f(\tilde{\mathbf{u}})_x = S(\tilde{\mathbf{u}}) \tag{5}$$

Subtracting (5) from (4) leads to,

$$\Delta\mathbf{u}_t + [f(\Delta\mathbf{u} + \tilde{\mathbf{u}}) - f(\tilde{\mathbf{u}})]_x = S(\Delta\mathbf{u} + \tilde{\mathbf{u}}) - S(\tilde{\mathbf{u}}). \tag{6}$$

But since $S(\tilde{\mathbf{u}})$ is a linear functional in terms of the conserved variables, then equation (6) simplifies to,

$$\Delta\mathbf{u}_t + [f(\Delta\mathbf{u} + \tilde{\mathbf{u}}) - f(\tilde{\mathbf{u}})]_x = S(\Delta\mathbf{u}). \tag{7}$$

Our proposed numerical scheme follows a classical finite volume construction; we start by defining the piecewise linear interpolants that approximate the exact solution $\mathbf{u}(x,t^n)$ on the cells C_i as follows:

$$\mathcal{L}_i(x,t^n) = \mathbf{u}_i^n + (x - x_i)(\mathbf{u}_i^n)', \qquad \forall x \in C_i$$

where $(\mathbf{u}_i^n)'$ is a limited numerical gradient approximating $\frac{\partial\mathbf{u}}{\partial x}(x_i,t^n)$ obtained using the (MC-θ) limiter. Next, we integrate (7) over the domain $R_{i+\frac{1}{2}}^n = D_{i+\frac{1}{2}} \times [t^n, t^{n+1}]$:

$$\iint_{R_{i+\frac{1}{2}}^n} \Delta\mathbf{u}_t + [f(\Delta\mathbf{u} + \tilde{\mathbf{u}}) - f(\tilde{\mathbf{u}})]_x dR = \iint_{R_{i+\frac{1}{2}}^n} S(\Delta\mathbf{u}) dR. \tag{8}$$

Applying Green's formula to the double integral on the left-hand side of equation (8) yields,

$$\Delta\mathbf{u}_{i+\frac{1}{2}}^{n+1} = \Delta\mathbf{u}_{i+\frac{1}{2}}^{n} - \frac{1}{\Delta x}\left[\int_{t^n}^{t^{n+1}} \left\{f((\Delta\mathbf{u}+\tilde{\mathbf{u}})(x_{i+1},t)) - f((\Delta\mathbf{u}+\tilde{\mathbf{u}})(x_i,t))\right\} dt\right] + \frac{\Delta t}{\Delta x} f(\tilde{\mathbf{u}}(x_{i+1})) - \frac{\Delta t}{\Delta x} f(\tilde{\mathbf{u}}(x_i)) + \frac{1}{\Delta x}\int_{t^n}^{t^{n+1}}\int_{x_i}^{x_{i+1}} S(\Delta\mathbf{u})dxdt. \quad (9)$$

The integrals in equation (9) should be approximated using second-order quadratures. The flux integrals are estimated using the midpoint quadrature rule as follows:

$$\int_{t^n}^{t^{n+1}} f((\Delta\mathbf{u}+\tilde{\mathbf{u}})(x_i,t))dt \approx f((\Delta\mathbf{u}+\tilde{\mathbf{u}})_i^{n+\frac{1}{2}})\Delta t,$$

$$\int_{t^n}^{t^{n+1}} f((\Delta\mathbf{u}+\tilde{\mathbf{u}})(x_{i+1},t))dt \approx f((\Delta\mathbf{u}+\tilde{\mathbf{u}})_{i+1}^{n+\frac{1}{2}})\Delta t.$$

Plugging these integrals in equation (9), leads to:

$$\Delta\mathbf{u}_{i+\frac{1}{2}}^{n+1} = \Delta\mathbf{u}_{i+\frac{1}{2}}^{n} - \frac{\Delta t}{\Delta x}[f(\Delta\mathbf{u}_{i+1}^{n+\frac{1}{2}} + \tilde{\mathbf{u}}_{i+1}) - f(\tilde{\mathbf{u}}_{i+1}) - f(\Delta\mathbf{u}_i^{n+\frac{1}{2}} + \tilde{\mathbf{u}}_i) + f(\tilde{\mathbf{u}}_i)] + \frac{1}{\Delta x}\int_{t^n}^{t^{n+1}}\int_{x_i}^{x_{i+1}} S(\Delta\mathbf{u})dxdt. \quad (10)$$

The forward projection step of $\Delta\mathbf{u}_i^n$ onto the staggered grid is calculated using Taylor expansion of $\Delta\mathbf{u}(x,t^n)$ in space:

$$\Delta\mathbf{u}_{i+\frac{1}{2}}^{n} = \frac{1}{2}(\Delta\mathbf{u}_i^n + \Delta\mathbf{u}_{i+1}^n) + \frac{\Delta x}{8}((\Delta\mathbf{u}_i^n)' - (\Delta\mathbf{u}_{i+1}^n)') \quad (11)$$

where $(\Delta\mathbf{u}_i^n)'$ is the derivative of $\Delta\mathbf{u}(x_i,t^n)$ calculated using the MC-θ limiter. The predicted values $\Delta\mathbf{u}_i^{n+\frac{1}{2}}$ appearing in equation (10) are obtained at the intermediate time $t^{n+\frac{1}{2}}$ using a first-order Taylor expansion in time and the balance law (7) as follows:

$$\Delta\mathbf{u}(x_i,t^{n+\frac{1}{2}}) \approx \Delta\mathbf{u}(x_i,t^n) + \frac{\Delta t}{2}\Delta\mathbf{u}_t(x_i,t^n),$$

$$\Delta\mathbf{u}_i^{n+\frac{1}{2}} \approx \Delta\mathbf{u}_i^n + \frac{\Delta t}{2}[-[f(\Delta\mathbf{u}+\tilde{\mathbf{u}}) - f(\tilde{\mathbf{u}})]_x|_{(x_i,t^n)} + [S(\Delta\mathbf{u})]|_{(x_i,t^n)}].$$

Hence we obtain

$$\Delta\mathbf{u}_i^{n+\frac{1}{2}} = \Delta\mathbf{u}_i^n + \frac{\Delta t}{2}[-(f_i^n)' + \tilde{f}_i{}' + S_i^n] \quad (12)$$

where $(f_i^n)'$ and $\tilde{f}_i{}'$ are the spacial numerical derivative of $f = f(\Delta u + \tilde{u})$ and $\tilde{f} = f(\tilde{u})$, respectively. S_i^n is the discretized source term at time t^n and is estimated as follows:

$$S_i^n = S(\Delta\mathbf{u})|_{(x_i,t^n)} = \begin{pmatrix} 0 \\ -\Delta\rho_i^n(\phi_x)_i \\ -\Delta\rho u_i^n(\phi_x)_i \end{pmatrix}.$$

On the other hand, the integral of the source term in (10) is discretized using the midpoint quadrature rule with respect to time and space:

$$\int_{t^n}^{t^{n+1}}\int_{x_i}^{x_{i+1}} S(\Delta\mathbf{u})dxdt \approx \Delta t\Delta x S(\Delta\mathbf{u}_i^{n+\frac{1}{2}}, \Delta\mathbf{u}_{i+1}^{n+\frac{1}{2}}),$$

with

$$S(\Delta\mathbf{u}_i^{n+\frac{1}{2}}, \Delta\mathbf{u}_{i+1}^{n+\frac{1}{2}}) = \begin{pmatrix} 0 \\ -(\phi_x)_i \frac{(\Delta\rho)_{i+1}^{n+\frac{1}{2}} + (\Delta\rho)_i^{n+\frac{1}{2}}}{2} \\ -(\phi_x)_i \frac{(\Delta\rho u)_{i+1}^{n+\frac{1}{2}} + (\Delta\rho u)_i^{n+\frac{1}{2}}}{2} \end{pmatrix}. \tag{13}$$

Finally, the projection step of $\Delta\mathbf{u}_{i+\frac{1}{2}}^{n+1}$ back onto the original grid is calculated using Taylor expansions in space:

$$\Delta\mathbf{u}_i^{n+1} = \frac{1}{2}(\Delta\mathbf{u}_{i-\frac{1}{2}}^{n+1} + \Delta\mathbf{u}_{i+\frac{1}{2}}^{n+1}) + \frac{\Delta x}{8}((\Delta\mathbf{u}_{i-\frac{1}{2}}^{n+1})' - (\Delta\mathbf{u}_{i+\frac{1}{2}}^{n+1})'). \tag{14}$$

Equation (14) is used to define the numerical solution of the Euler with gravity system. To complete the presentation of the one-dimensional scheme, we still need to show that it is capable of capturing any stationary solution up to machine accuracy. Without any loss of generality, we assume that the updated solution satisfies $\mathbf{u}_i^n = \tilde{\mathbf{u}}_i$, i.e., $\Delta\mathbf{u}_i^n = 0$ at time $t = t^n$. Performing one iteration using the proposed numerical scheme, one can show that:

1. $\Delta\mathbf{u}_i^{n+\frac{1}{2}} = 0$.
2. $\Delta\mathbf{u}_{i+\frac{1}{2}}^{n+1} = 0$.
3. $\Delta\mathbf{u}_i^{n+1} = 0$.

The proof of 2 and 3 follows immediately after 1 is established. We start by showing 1.
$f(\Delta\mathbf{u} + \tilde{\mathbf{u}})$ is given by,

$$f(\Delta\mathbf{u} + \tilde{\mathbf{u}}) = \begin{pmatrix} \Delta\rho u + \tilde{\rho} u \\ \frac{(\Delta\rho u + \tilde{\rho} u)^2}{\Delta\rho + \tilde{\rho}} + (\gamma - 1)[\Delta E + \tilde{E} - \frac{1}{2}\frac{(\Delta\rho u + \tilde{\rho} u)^2}{\Delta\rho + \tilde{\rho}}] \\ \left[\Delta E + \tilde{E} + (\gamma - 1)(\Delta E + \tilde{E} - \frac{1}{2}\frac{(\Delta\rho u + \tilde{\rho} u)^2}{\Delta\rho + \tilde{\rho}})\right](\frac{\Delta\rho u + \tilde{\rho} u}{\Delta\rho + \tilde{\rho}}) \end{pmatrix}.$$

The prediction step leads to,

$$\Delta\mathbf{u}_i^{n+\frac{1}{2}} = \Delta\mathbf{u}_i^n + \frac{\Delta t}{2}[-\frac{f'(\Delta\mathbf{u}_i^n + \tilde{\mathbf{u}}_i)}{\Delta x} + \frac{f'(\tilde{\mathbf{u}}_i)}{\Delta x} + S(\Delta\mathbf{u}_i^n)]. \tag{15}$$

But since $\Delta\mathbf{u}_i^n = 0$, then we obtain,

$$\Delta\mathbf{u}_i^{n+\frac{1}{2}} = \frac{\Delta t}{2}\left[-\frac{f'(\tilde{\mathbf{u}}_i)}{\Delta x} + \frac{f'(\tilde{\mathbf{u}}_i)}{\Delta x}\right].$$

Hence, $\Delta\mathbf{u}_i^{n+\frac{1}{2}} = 0$; the proof of points 2 and 3 follows immediately. We conclude that the updated numerical solution $\mathbf{u}_i^{n+1}$ remains stationary up to machine precision.

2.3. TVD property of the UCS scheme with the subtraction method in the scalar case

In this section we establish the TVD property of our proposed numerical schemes. Let the scalar conservation law,

$$u_t + f(u)_x = 0. \tag{16}$$

In the context of the subtraction method, we will discretize the equation,

$$\Delta u_t + h(\Delta u)_x = 0, \tag{17}$$

where $\Delta u = u - \tilde{u}$ and $h(\Delta u) = f(\Delta u + \tilde{u}) - f(\tilde{u})$. $\tilde{u}$ a time independent reference solution. Using our UCS base scheme, the numerical solution of the scalar equation (17) is updated at time t^{n+1} as follows: First, we apply a forward projection step,

$$\Delta u_{i+\frac{1}{2}}^n = \frac{1}{2}\left(\Delta u_i^n + \Delta u_{i+1}^n\right) + \frac{\Delta x}{8}\left(\left(\Delta u_i^n\right)' - \left(\Delta u_{i+1}^n\right)'\right). \tag{18}$$

Then, we predict the solution values at time $t^{n+\frac{1}{2}}$ with a aid of the predictor step,

$$\Delta u_i^{n+\frac{1}{2}} = \Delta u_i^n + \frac{\Delta t}{2}[(h_i^n)']. \tag{19}$$

Next, we apply the time evolution step

$$\Delta u_{i+\frac{1}{2}}^{n+1} = \Delta u_{i+\frac{1}{2}}^{n} - \lambda \left[h(\Delta u_{i+1}^{n+\frac{1}{2}}) - h(\Delta u_{i}^{n+\frac{1}{2}}) \right]. \tag{20}$$

Finally, we apply the backward projection step

$$\Delta u_{i}^{n+1} = \frac{1}{2}\left(\Delta u_{i-\frac{1}{2}}^{n+1} + \Delta u_{i+\frac{1}{2}}^{n+1}\right) + \frac{\Delta x}{8}\left(\left(\Delta u_{i-\frac{1}{2}}^{n+1}\right)' - \left(\Delta u_{i+\frac{1}{2}}^{n+1}\right)'\right). \tag{21}$$

Theorem 1. *Assume that the numerical spatial derivatives be chosen as in [17],*

$$0 \le \Delta u_i'.sgn(\Delta u_{i+1} - \Delta u_i) \le Cst_{\Delta u}.\left| minmod\left(\frac{\Delta u_{i+1} - \Delta u_i}{\Delta x}, \frac{\Delta u_i - \Delta u_{i-1}}{\Delta x}\right)\right|,$$

$$0 \le h_i'.sgn(\Delta u_{i+1} - \Delta u_i) \le Cst_{h}.\left| minmod\left(\frac{\Delta u_{i+1} - \Delta u_i}{\Delta x}, \frac{\Delta u_i - \Delta u_{i-1}}{\Delta x}\right)\right|,$$

with $Cst_{\Delta u} = \alpha$ and the following CFL condition holds,

$$\lambda.max|a(u_i)| \le \beta$$

where

$$\beta = \lambda \frac{Cst_f}{Cst_{\Delta u}} \le \frac{\sqrt{4 + 4\alpha - \alpha^2} - 2}{2\alpha},$$

and $\alpha < 4$ (for $\beta > 0$). Then the scheme satisfies the TVD property.

Proof. Inspired by the TVD proof in [17] and [12], one can say that it is enough to prove that $|A_i| \le \frac{1}{2}$ and $|C_{i+\frac{1}{2}}| \le \frac{1}{2}$ with $A_i = \frac{\frac{\Delta x}{8}\left(\left(\Delta u_{i-\frac{1}{2}}^{n+1}\right)' - \left(\Delta u_{i+\frac{1}{2}}^{n+1}\right)'\right)}{\left(\Delta u_{i+\frac{1}{2}}^{n+1} - \Delta u_{i-\frac{1}{2}}^{n+1}\right)}$ and $C_{i+\frac{1}{2}} = \frac{\lambda\left[h(\Delta u_{i+1}^{n+\frac{1}{2}}) - h(\Delta u_{i}^{n+\frac{1}{2}})\right] - \frac{\Delta x}{8}\left((\Delta u_i^n)' - \left(\Delta u_{i+1}^n\right)'\right)}{\Delta u_{i+1}^n - \Delta u_i^n}$.

First we show that $|A_i| \le \frac{1}{2}$,

$$\frac{\Delta x}{8}\left|\frac{\left(\Delta u_{i-\frac{1}{2}}^{n+1}\right)' - \left(\Delta u_{i+\frac{1}{2}}^{n+1}\right)'}{\left(\Delta u_{i+\frac{1}{2}}^{n+1} - \Delta u_{i-\frac{1}{2}}^{n+1}\right)}\right| \le \frac{\Delta x}{8}\max\left(\left|\frac{\left(\Delta u_{i-\frac{1}{2}}^{n+1}\right)'}{\left(\Delta u_{i+\frac{1}{2}}^{n+1} - \Delta u_{i-\frac{1}{2}}^{n+1}\right)}\right|, \left|\frac{\left(\Delta u_{i+\frac{1}{2}}^{n+1}\right)'}{\left(\Delta u_{i+\frac{1}{2}}^{n+1} - \Delta u_{i-\frac{1}{2}}^{n+1}\right)}\right|\right) \le \frac{\alpha}{8} \le \frac{1}{2}. \tag{22}$$

Next we show that $|C_{i+\frac{1}{2}}| \le \frac{1}{2}$,

$$\begin{aligned}
&\left|\frac{\lambda\left[h(\Delta u_{i+1}^{n+\frac{1}{2}}) - h(\Delta u_{i}^{n+\frac{1}{2}})\right] - \frac{\Delta x}{8}\left((\Delta u_i^n)' - \left(\Delta u_{i+1}^n\right)'\right)}{\Delta u_{i+1}^n - \Delta u_i^n}\right| \\
&\qquad \le \lambda\left|\frac{h(\Delta u_{i+1}^{n+\frac{1}{2}}) - h(\Delta u_{i}^{n+\frac{1}{2}})}{\Delta u_{i+1}^n - \Delta u_i^n}\right| + \frac{\Delta x}{8}\left|\frac{(\Delta u_i^n)' - \left(\Delta u_{i+1}^n\right)'}{\Delta u_{i+1}^n - \Delta u_i^n}\right| \\
&\qquad \le \lambda\left|\frac{h(\Delta u_{i+1}^{n+\frac{1}{2}}) - h(\Delta u_{i}^{n+\frac{1}{2}})}{\Delta u_{i+1}^{n+\frac{1}{2}} - \Delta u_i^{n+\frac{1}{2}}}\right| \cdot \left|\frac{\Delta u_{i+1}^{n+\frac{1}{2}} - \Delta u_i^{n+\frac{1}{2}}}{\Delta u_{i+1}^n - \Delta u_i^n}\right| + \frac{\Delta x}{8}\left|\frac{(\Delta u_i^n)' - \left(\Delta u_{i+1}^n\right)'}{\Delta u_{i+1}^n - \Delta u_i^n}\right|
\end{aligned} \tag{23}$$

From the CFL condition one concludes that,

$$\lambda\left|\frac{h(\Delta u_{i+1}^{n+\frac{1}{2}}) - h(\Delta u_{i}^{n+\frac{1}{2}})}{\Delta u_{i+1}^{n+\frac{1}{2}} - \Delta u_i^{n+\frac{1}{2}}}\right| \le \beta. \tag{24}$$

Next, from the predictor step $u_i^{n+\frac{1}{2}}$, the second absolute value to the right-hand side of inequality (23) is bounded by

$$\left|\frac{\Delta u_{i+1}^{n+\frac{1}{2}}-\Delta u_i^{n+\frac{1}{2}}}{\Delta u_{i+1}^n-\Delta u_i^n}\right| = \left|\frac{\Delta u_{i+1}^n-\frac{\Delta t}{2}h'_{i+1}-\Delta u_i^n+\frac{\Delta t}{2}h'_i}{\Delta u_{i+1}^n-\Delta u_i^n}\right| = \left|\frac{\Delta u_{i+1}^n-\Delta u_i^n-\frac{\Delta t}{2}(h'_{i+1}-h'_i)}{\Delta u_{i+1}^n-\Delta u_i^n}\right|$$
$$\leq 1+\frac{\Delta t}{2}\left|\frac{h'_{i+1}-h'_i}{\Delta u_{i+1}^n-\Delta u_i^n}\right| \leq 1+\frac{\Delta t}{2}\max\left(\left|\frac{h'_{i+1}}{\Delta u_{i+1}^n-\Delta u_i^n}\right|,\left|\frac{h'_i}{\Delta u_{i+1}^n-\Delta u_i^n}\right|\right)$$
$$\leq 1+\frac{\lambda}{2}Cst_h \leq 1+\frac{\alpha\beta}{2}. \quad (25)$$

Finally, we have

$$\frac{\Delta x}{8}\left|\frac{\left(\Delta u_i^n\right)'-\left(\Delta u_{i+1}^n\right)'}{\Delta u_{i+1}^n-\Delta u_i^n}\right| \leq \frac{\Delta x}{8}\max\left(\left|\frac{\left(\Delta u_{i+1}^n\right)'}{\Delta u_{i+1}^n-\Delta u_i^n}\right|,\left|\frac{\left(\Delta u_i^n\right)'}{\Delta u_{i+1}^n-\Delta u_i^n}\right|\right) \leq \frac{\alpha}{8}. \quad (26)$$

Performing the following term-by-term operations, (24)×(25)+(26) result in,

$$\left|\frac{\lambda\left[h(\Delta u_{i+1}^{n+\frac{1}{2}})-h(\Delta u_i^{n+\frac{1}{2}})\right]-\frac{\Delta x}{8}\left(\left(\Delta u_i^n\right)'-\left(\Delta u_{i+1}^n\right)'\right)}{\Delta u_{i+1}^n-\Delta u_i^n}\right| \leq \beta(1+\frac{1}{2}\alpha\beta)+\frac{1}{8}\alpha \leq \frac{1}{2}. \quad (27)$$

This follows from the definition of β, and we conclude that,

$$|C_{i+\frac{1}{2}}| \leq \frac{1}{2}. \quad (28)$$

The total variation in the updated solution is now,

$$\begin{aligned}
TV(\Delta u(t+\Delta t)) &= \sum_i |\Delta u_{i+1}(t+\Delta t)-\Delta u_i(t+\Delta t)|,\\
&\leq \sum_i \left|\Delta u_{i+\frac{3}{2}}^{n+1}-\Delta u_{i+\frac{1}{2}}^{n+1}\right|\left|\frac{1}{2}+A_{i+1}\right|+\left|\Delta u_{i+\frac{1}{2}}^{n+1}-\Delta u_{i-\frac{1}{2}}^{n+1}\right|\left|\frac{1}{2}-A_i\right|,\\
&= \sum_i \left|\Delta u_{i+\frac{1}{2}}^{n+1}-\Delta u_{i-\frac{1}{2}}^{n+1}\right|,\\
&\leq \sum_i \left|\Delta u_{i+1}^n-\Delta u_i^n\right|\left|\frac{1}{2}-C_{i+\frac{1}{2}}\right|+\left|\Delta u_{i+1}^n-\Delta u_i^n\right|\left|\frac{1}{2}+C_{i-\frac{1}{2}}\right|,\\
&= \sum_i \left|\Delta u_{i+1}^n-\Delta u_i^n\right| = \sum_i |\Delta u_{i+1}(t)-\Delta u_i(t)| = TV(\Delta u(t)),
\end{aligned}$$

here we followed a re-indexing step twice. We conclude that

$$\begin{aligned}
TV(u(t+\Delta t))-TV(u(t)) &= TV(\Delta u(t+\Delta t)+\tilde{u})-TV(\Delta u(t)+\tilde{u}),\\
&\leq TV(\Delta u(t+\Delta t))+TV(\tilde{u})-TV(\Delta u(t))-TV(\tilde{u}),\\
&= TV(\Delta u(t+\Delta t))-TV(\Delta u(t)) \leq 0,
\end{aligned}$$

hence,

$$TV(u(t+\Delta t)) \leq TV(u(t)). \quad \square$$

Thanks to Theorem 1 we can claim that our proposed numerical scheme satisfies the TVD property in the case of a scalar conservation law, and thus insures the convergence of the numerical solution to a weak solution of the conservation law.

3. Unstaggered well-balanced central scheme for the two-dimensional Euler system with gravity

In this section we extend the proposed well-balanced scheme we derived in section 2 to the case of the two-dimensional Euler with gravity systems, using a reconstruction technique similar to the one proposed in [4]. The well-balanced property of the proposed two-dimensional scheme is presented at the end of this section.

3.1. Two-dimensional Euler system with gravity

We consider the two-dimensional Euler system with gravity:

$$\begin{cases} \mathbf{U}_t + F(\mathbf{U})_x + G(\mathbf{U})_y = S(\mathbf{U}), \qquad (x, y) \in \Omega \subset \mathbb{R}^2, \ t > 0. \\ \mathbf{U}(x, y, 0) = \mathbf{U}_0(x, y), \end{cases} \tag{29}$$

where

$$\mathbf{U} = \begin{pmatrix} \rho \\ \rho u \\ \rho v \\ E \end{pmatrix}, \ F(\mathbf{U}) = \begin{pmatrix} \rho u \\ \rho u^2 + p \\ \rho uv \\ (E + p)u \end{pmatrix}, \ G(\mathbf{U}) = \begin{pmatrix} \rho v \\ \rho uv \\ \rho v^2 + p \\ (E + p)v \end{pmatrix},$$

and

$$S(\mathbf{u}) = \begin{pmatrix} 0 \\ -\rho\phi_x \\ -\rho\phi_y \\ -\rho u\phi_x - \rho v\phi_y \end{pmatrix}$$

Here ρ is the fluid density, u and v are the velocities in the x and y-direction respectively, p is the pressure and $E = \frac{1}{2}\rho(u^2 + v^2) + \frac{p}{\gamma-1}$ is the non-gravitational energy which includes the kinetic and internal energy of the fluid. The gravitational potential $\phi = \phi(x, y)$ is a given function and γ is the ratio of specific heats. Similarly to the one-dimensional case and in absence of gravity the Euler with gravity system reduces to a hyperbolic system of conservation laws with real eigenvalues and a complete set of linearly independent eigenvectors.

3.2. The two-dimensional unstaggered FV central scheme

We consider a Cartesian domain decomposition of the computational domain Ω where the control cells are the rectangles $C_{i,j} = \left[x_{i-\frac{1}{2}}, x_{i+\frac{1}{2}}\right] \times \left[y_{j-\frac{1}{2}}, y_{j+\frac{1}{2}}\right]$ centered at the nodes (x_i, y_j). We define the dual staggered cells $D_{i+\frac{1}{2},j+\frac{1}{2}} = [x_i, x_{i+1}] \times \left[y_j, y_{j+1}\right]$ centered at $(x_{i+\frac{1}{2}}, y_{j+\frac{1}{2}})$ where $x_{i+\frac{1}{2}} = x_i + \frac{\Delta x}{2}$ and $y_{j+\frac{1}{2}} = y_j + \frac{\Delta y}{2}$, where $\Delta x = x_{i+\frac{1}{2}} - x_{i-\frac{1}{2}}$ and $\Delta y = y_{j+\frac{1}{2}} - y_{j-\frac{1}{2}}$.

Before proceeding with the derivation of the two-dimensional numerical, and for convenience, we need to introduce the average value notations:

$$\overline{\rho}_{i,j+\frac{1}{2}} = \frac{\rho_{i,j} + \rho_{i,j+1}}{2}, \overline{\rho}_{i+\frac{1}{2},j} = \frac{\rho_{i,j} + \rho_{i+1,j}}{2}, \overline{\rho}_{i,(j)} = \frac{\rho_{i,j+\frac{1}{2}} + \rho_{i,j-\frac{1}{2}}}{2}$$
$$\overline{\rho}_{(i),j} = \frac{\rho_{i+\frac{1}{2},j} + \rho_{i-\frac{1}{2},j}}{2}, \quad [[\rho]]_{i,j+\frac{1}{2}} = \rho_{i,j+1} - \rho_{i,j}$$
$$[[\rho]]_{i+\frac{1}{2},j} = \rho_{i+1,j} - \rho_{i,j}, \ [[\rho]]_{i,(j)} = \rho_{i,j+\frac{1}{2}} - \rho_{i,j-\frac{1}{2}}, \ [[\rho]]_{(i),j} = \rho_{i+\frac{1}{2},j} - \rho_{i-\frac{1}{2},j}.$$

We follow the same strategy we considered in section 2; we assume that $\tilde{\mathbf{U}}$ is a given stationary solution of system (29) and we define $\Delta\mathbf{U} = \mathbf{U} - \tilde{\mathbf{U}}$. We substitute $\mathbf{U} = \Delta\mathbf{U} + \tilde{\mathbf{U}}$ in the balance law (29), we obtain:

$$\Delta\mathbf{U}_t + F(\Delta\mathbf{U} + \tilde{\mathbf{U}})_x + G(\Delta\mathbf{U} + \tilde{\mathbf{U}})_y = S(\Delta\mathbf{U} + \tilde{\mathbf{U}}). \tag{30}$$

On the other hand, since $\tilde{\mathbf{U}}$ is a stationary solution, then balance law in (29) reduces to

$$F(\tilde{\mathbf{U}})_x + G(\tilde{\mathbf{U}})_y = S(\tilde{\mathbf{U}}). \tag{31}$$

Subtracting equation (31) from equation (30), we obtain

$$\Delta\mathbf{U}_t + [F(\Delta\mathbf{U} + \tilde{\mathbf{U}}) - F(\tilde{\mathbf{U}})]_x + [G(\Delta\mathbf{U} + \tilde{\mathbf{U}}) - G(\tilde{\mathbf{U}})]_y = S(\Delta\mathbf{U} + \tilde{\mathbf{U}}) - S(\tilde{\mathbf{U}}). \tag{32}$$

Using the fact that the source term $S(\mathbf{U})$ in equation (29) is linear in terms of the conserved variables, then equation (32) reduces to

$$\Delta\mathbf{U}_t + [F(\Delta\mathbf{U} + \tilde{\mathbf{U}}) - F(\tilde{\mathbf{U}})]_x + [G(\Delta\mathbf{U} + \tilde{\mathbf{U}}) - G(\tilde{\mathbf{U}})]_y = S(\Delta\mathbf{U}). \tag{33}$$

The proposed numerical scheme consists of evolving the balance law in equation (33) instead on evolving the balance law in system (29). The numerical solution $\mathbf{U}$ will be then obtained using the formula $\mathbf{U} = \Delta\mathbf{U} + \tilde{\mathbf{U}}$. The numerical scheme that we

shall use to evolve $\Delta\mathbf{U}(x,y,t)$ follows a classical finite volume approach; it evolves a piecewise linear function $\mathcal{L}_{i,j}(x,y,t)$ defined on the control cells $C_{i,j}$ and used to approximate the analytic solution $\mathbf{U}(x,y,t)$ of system (29). Without any loss of generality we can assume that $\mathbf{U}^n_{i,j}$ is known at time t^n and we define $\mathcal{L}_{i,j}(x,y,t^n)$ on the cells $C_{i,j}$ as follows.

$$\mathcal{L}_{i,j}(x,y,t^n) = \mathbf{U}^n_{i,j} + (x-x_i)\frac{(\mathbf{U}^n_{i,j})'}{\Delta x} + (y-y_j)\frac{(\mathbf{U}^n_{i,j})'}{\Delta y}, \qquad \forall (x,y) \in C_{i,j},$$

where $\frac{(\mathbf{U}^n_{i,j})'}{\Delta x}$ and $\frac{(\mathbf{U}^n_{i,j})'}{\Delta y}$ are limited numerical gradients approximating $\frac{\partial \mathbf{U}}{\partial x}$ and $\frac{\partial \mathbf{U}}{\partial y}$, respectively, at the point (x_i, y_j, t^n). The (MC-θ) limiter is used to avoid spurious oscillations. Next we integrate the balance law in (33) on the rectangular box $R^n_{i+\frac{1}{2},j+\frac{1}{2}} = D_{i+\frac{1}{2},j+\frac{1}{2}} \times [t^n, t^{n+1}]$,

$$\iiint\limits_{R_{i+\frac{1}{2},j+\frac{1}{2}}} \Delta\mathbf{U}_t + [F(\Delta\mathbf{U}+\tilde{\mathbf{U}}) - F(\tilde{\mathbf{U}})]_x + [G(\Delta\mathbf{U}+\tilde{\mathbf{U}}) - G(\tilde{\mathbf{U}})]_y dR = \iiint\limits_{R_{i+\frac{1}{2},j+\frac{1}{2}}} S(\Delta\mathbf{U}) dR. \tag{34}$$

Next we use the fact that $\Delta\mathbf{U}$ is approximated using piecewise linear interpolants similar to $\mathcal{L}_{i,j}$ on the cells $C_{i,j}$; following the derivation of the unstaggered central schemes in [19], equation (34) is rewritten as:

$$\Delta\mathbf{U}^{n+1}_{i+\frac{1}{2},j+\frac{1}{2}} = \Delta\mathbf{U}^n_{i+\frac{1}{2},j+\frac{1}{2}} - \frac{1}{\Delta x\Delta y} \iiint\limits_{R_{i+\frac{1}{2},j+\frac{1}{2}}} [F(\Delta\mathbf{U}+\tilde{\mathbf{U}}) - F(\tilde{\mathbf{U}})]_x + [G(\Delta\mathbf{U}+\tilde{\mathbf{U}}) - G(\tilde{\mathbf{U}})]_y dR + \frac{1}{\Delta x\Delta y} \iiint\limits_{R_{i+\frac{1}{2},j+\frac{1}{2}}} S(\Delta\mathbf{U}) dR. \tag{35}$$

The flux integrals in equation (35) are calculated using the divergence theorem. Let n_x, n_y denote the normal unit vectors in the $x-$ and $y-$ directions, respectively. Therefore we obtain:

$$\Delta\mathbf{U}^{n+1}_{i+\frac{1}{2},j+\frac{1}{2}} = \Delta\mathbf{U}^n_{i+\frac{1}{2},j+\frac{1}{2}} - \frac{1}{\Delta x\Delta y} \int_{t^n}^{t^{n+1}} \int_{\partial R} [F(\Delta\mathbf{U}+\tilde{\mathbf{U}}) - F(\tilde{\mathbf{U}})]_x . n_x dS dt - \int_{t^n}^{t^{n+1}} \int_{\partial R} [G(\Delta\mathbf{U}+\tilde{\mathbf{U}}) - G(\tilde{\mathbf{U}})]_y . n_y dS dt + \frac{1}{\Delta x\Delta y} \iiint\limits_{R_{i+\frac{1}{2},j+\frac{1}{2}}} S(\Delta\mathbf{U}) dR. \tag{36}$$

The forward projection step in equation (36) consists of projecting the solution at time t^n onto the staggered grid and it is performed using linear interpolation in two space dimensions in addition to Taylor expansions in space; we obtain:

$$\Delta\mathbf{U}^n_{i+\frac{1}{2},j+\frac{1}{2}} = \frac{1}{2}(\overline{\Delta\mathbf{U}}^n_{i+\frac{1}{2},j} + \overline{\Delta\mathbf{U}}^n_{i+\frac{1}{2},j+1}) - \frac{\Delta x}{16}([[\Delta\mathbf{U}^{n,x}]]_{i+\frac{1}{2},j} + [[\Delta\mathbf{U}^{n,x}]]_{i+\frac{1}{2},j+1}) - \frac{\Delta y}{16}([[\Delta\mathbf{U}^{n,y}]]_{i,j+\frac{1}{2}} + [[\Delta\mathbf{U}^{n,y}]]_{i+1,j+\frac{1}{2}}). \tag{37}$$

The integral of the source term is being approximated using the midpoint quadrature rule both in time and space:

$$\iiint\limits_{R_{i+\frac{1}{2},j+\frac{1}{2}}} S(\Delta\mathbf{U}) dR = \Delta x\Delta y\Delta t . S(\Delta\mathbf{U}^{n+\frac{1}{2}}_{i,j}, \Delta\mathbf{U}^{n+\frac{1}{2}}_{i+1,j}, \Delta\mathbf{U}^{n+\frac{1}{2}}_{i,j+1}, \Delta\mathbf{U}^{n+\frac{1}{2}}_{i+1,j+1}), \tag{38}$$

where,

$$S(\Delta\mathbf{U}^{n+\frac{1}{2}}_{i,j}, \Delta\mathbf{U}^{n+\frac{1}{2}}_{i+1,j}, \Delta\mathbf{U}^{n+\frac{1}{2}}_{i,j+1}, \Delta\mathbf{U}^{n+\frac{1}{2}}_{i+1,j+1}) = (S_1, S_2, S_3, S_4)$$

with

$$S_1 = 0$$

$$S_2 = -(\phi_x)_{i,j}[\frac{(\Delta\rho)^{n+\frac{1}{2}}_{i+1,j+1} + (\Delta\rho)^{n+\frac{1}{2}}_{i+1,j} + (\Delta\rho)^{n+\frac{1}{2}}_{i,j+1} + (\Delta\rho)^{n+\frac{1}{2}}_{i,j}}{2}]$$

$$S_3 = -(\phi_y)_{i,j}[\frac{(\Delta\rho)^{n+\frac{1}{2}}_{i+1,j+1} + (\Delta\rho)^{n+\frac{1}{2}}_{i+1,j} + (\Delta\rho)^{n+\frac{1}{2}}_{i,j+1} + (\Delta\rho)^{n+\frac{1}{2}}_{i,j}}{2}]$$

$$S_4 = -(\phi_x)_{i,j}[\frac{(\Delta\rho u)^{n+\frac{1}{2}}_{i+1,j+1} + (\Delta\rho u)^{n+\frac{1}{2}}_{i+1,j} + (\Delta\rho u)^{n+\frac{1}{2}}_{i,j+1} + (\Delta\rho u)^{n+\frac{1}{2}}_{i,j}}{2}]$$
$$- (\phi_y)_{i,j}[\frac{(\Delta\rho v)^{n+\frac{1}{2}}_{i+1,j+1} + (\Delta\rho v)^{n+\frac{1}{2}}_{i+1,j} + (\Delta\rho v)^{n+\frac{1}{2}}_{i,j+1} + (\Delta\rho v)^{n+\frac{1}{2}}_{i,j}}{2}]$$

Finally, the evolution step at time t^{n+1} at the staggered nodes can be written as,

$$\begin{aligned}\Delta\mathbf{U}^{n+1}_{i+\frac{1}{2},j+\frac{1}{2}} &= \Delta\mathbf{U}^{n}_{i+\frac{1}{2},j+\frac{1}{2}} \\ &- \frac{\Delta t}{2}[D^x_+ F(\Delta\mathbf{U}^{n+\frac{1}{2}}_{i,j} + \tilde{\mathbf{U}}_{i,j}) - D^x_+ F(\tilde{\mathbf{U}}_{i,j}) + D^x_+ F(\Delta\mathbf{U}^{n+\frac{1}{2}}_{i,j+1} + \tilde{\mathbf{U}}_{i,j+1}) - D^x_+ F(\tilde{\mathbf{U}}_{i,j+1})] \\ &- \frac{\Delta t}{2}[D^y_+ G(\Delta\mathbf{U}^{n+\frac{1}{2}}_{i,j} + \tilde{\mathbf{U}}_{i,j}) - D^y_+ G(\tilde{\mathbf{U}}_{i,j}) + D^y_+ F(\Delta\mathbf{U}^{n+\frac{1}{2}}_{i+1,j} + \tilde{\mathbf{U}}_{i+1,j}) - D^y_+ G(\tilde{\mathbf{U}}_{i+1,j})] \\ &+ \Delta t.S(\Delta\mathbf{U}^{n+\frac{1}{2}}_{i,j}, \Delta\mathbf{U}^{n+\frac{1}{2}}_{i+1,j}, \Delta\mathbf{U}^{n+\frac{1}{2}}_{i,j+1}, \Delta\mathbf{U}^{n+\frac{1}{2}}_{i+1,j+1}). \quad (39)\end{aligned}$$

Here D^x_+ and D^y_+ are the forward differences given by,
$D^x_+ F(\mathbf{U}_{i,j}) = \frac{F(\mathbf{U}_{i+1,j}) - F(\mathbf{U}_{i,j})}{\Delta x}$, $D^y_+ F(\mathbf{U}_{i,j}) = \frac{F(\mathbf{U}_{i,j+1}) - F(\mathbf{U}_{i,j})}{\Delta y}$.
The predicted values in equation (39) are generated at time $t^{n+\frac{1}{2}}$ using a first order Taylor's expansion in time in addition to the balance law (33):

$$\Delta\mathbf{U}^{n+\frac{1}{2}}_{i,j} = \Delta\mathbf{U}^{n}_{i,j} + \frac{\Delta t}{2}\left[-\frac{(F^n_{i,j})'}{\Delta x} + \frac{\tilde{F}'_{i,j}}{\Delta x} - \frac{(G^n_{i,j})'}{\Delta y} + \frac{\tilde{G}'_{i,j}}{\Delta y} + S^n_{i,j}\right], \quad (40)$$

where $\frac{(F^n_{i,j})'}{\Delta x}$, $\frac{\tilde{F}'_{i,j}}{\Delta x}$, $\frac{(G^n_{i,j})'}{\Delta y}$ and $\frac{\tilde{G}'_{i,j}}{\Delta y}$ denote the approximate spatial partial of $\tilde{F} = F(\tilde{U})$, $F = F(\Delta U + \tilde{U})$, $\tilde{G} = G(\tilde{U})$, and $G = G(\Delta U + \tilde{U})$ respectively. Here also we limit the spatial numerical derivatives using the MC-θ limiter to avoid spurious oscillations.

Finally we apply a back projection step similar to the one in (37) in order to retrieve the solution at the time t^{n+1} on the original cells $C_{i,j}$.

$$\begin{aligned}\Delta\mathbf{U}^{n+1}_{i,j} = \frac{1}{2}(\overline{\Delta\mathbf{U}}^{n+1}_{i,j-\frac{1}{2}} + \overline{\Delta\mathbf{U}}^{n+1}_{i,j+\frac{1}{2}}) - \frac{\Delta x}{16}([[\Delta\mathbf{U}^{n+1,x}]]_{(i),j-\frac{1}{2}} + [[\Delta\mathbf{U}^{n+1,x}]]_{(i),j+\frac{1}{2}}) \\ - \frac{\Delta y}{16}([[\Delta\mathbf{U}^{n+1,y}]]_{i-\frac{1}{2},(j)} + [[\Delta\mathbf{U}^{n+1,y}]]_{i+\frac{1}{2},(j)}), \quad (41)\end{aligned}$$

where $\Delta\mathbf{U}^{n+1,x}_{i,j}$ and $\Delta\mathbf{U}^{n+1,y}_{i,j}$ denote the spatial partial derivatives of the numerical solution obtained at time t^{n+1} and node (x_i, y_j) approximated using a limited numerical gradient.

To complete the presentation of the numerical scheme we need to verify the well-balanced property of the proposed scheme and to show that it is capable of maintaining stationary solutions of the Euler with gravity system.

Suppose that the numerical solution obtained at time $t = t^n$ satisfies $\mathbf{U}^n_{i,j} = \tilde{\mathbf{U}}_{i,j}$, i.e., $\Delta\mathbf{U}^n_{i,j} = 0$. Performing one iteration using the proposed numerical scheme, one can show that:

1. $\Delta\mathbf{U}^{n+\frac{1}{2}}_{i,j} = 0$.
2. $\Delta\mathbf{U}^{n+1}_{i+\frac{1}{2},j+\frac{1}{2}} = 0$.
3. $\Delta\mathbf{U}^{n+1}_{i,j} = 0$.

In fact, it is straight forward to establish 2 and 3 once 1 is established. We will present the proof of 1.
$F(\Delta\mathbf{U} + \tilde{\mathbf{U}})$ and $G(\Delta\mathbf{U} + \tilde{\mathbf{U}})$ are given by

$$F(\Delta\mathbf{U} + \tilde{\mathbf{U}}) = \begin{pmatrix} \Delta\rho u + \tilde{\rho}\tilde{u} \\ \frac{(\Delta\rho u + \tilde{\rho}\tilde{u})^2}{\Delta\rho + \tilde{\rho}} + (\gamma - 1)[\Delta E + \tilde{E} - \frac{1}{2}\frac{(\Delta\rho u + \tilde{\rho}\tilde{u})^2}{\Delta\rho + \tilde{\rho}} - \frac{1}{2}\frac{(\Delta\rho v + \tilde{\rho}\tilde{v})^2}{\Delta\rho + \tilde{\rho}}] \\ (\Delta\rho u + \tilde{\rho}\tilde{u})(\frac{\Delta\rho v + \tilde{\rho}\tilde{v}}{\Delta\rho + \tilde{\rho}}) \\ (\Delta E + \tilde{E} + (\gamma - 1)(\Delta E + \tilde{E} - \frac{1}{2}\frac{(\Delta\rho u + \tilde{\rho}\tilde{u})^2}{\Delta\rho + \tilde{\rho}} - \frac{1}{2}\frac{(\Delta\rho v + \tilde{\rho}\tilde{v})^2}{\Delta\rho + \tilde{\rho}})(\frac{\Delta\rho u + \tilde{\rho}\tilde{u}}{\Delta\rho + \tilde{\rho}}) \end{pmatrix}$$

and

$$G(\Delta\mathbf{U}+\tilde{\mathbf{U}}) = \begin{pmatrix} \Delta\rho v + \tilde{\rho v} \\ (\Delta\rho u + \tilde{\rho u})(\frac{\Delta\rho v+\tilde{\rho v}}{\Delta\rho+\tilde{\rho}}) \\ \frac{(\Delta\rho v+\tilde{\rho v})^2}{\Delta\rho+\tilde{\rho}} + (\gamma-1)[\Delta E + \tilde{E} - \frac{1}{2}\frac{(\Delta\rho u+\tilde{\rho u})^2}{\Delta\rho+\tilde{\rho}} - \frac{1}{2}\frac{(\Delta\rho v+\tilde{\rho v})^2}{\Delta\rho+\tilde{\rho}}] \\ (\Delta E + \tilde{E} + (\gamma-1)(\Delta E + \tilde{E} - \frac{1}{2}\frac{(\Delta\rho u+\tilde{\rho u})^2}{\Delta\rho+\tilde{\rho}} - \frac{1}{2}\frac{(\Delta\rho v+\tilde{\rho v})^2}{\Delta\rho+\tilde{\rho}})(\frac{\Delta\rho u+\tilde{\rho u}}{\Delta\rho+\tilde{\rho}}) \end{pmatrix}$$

The prediction step leads to

$$\Delta\mathbf{U}_{i,j}^{n+\frac{1}{2}} = \Delta\mathbf{U}_{i,j}^{n} + \frac{\Delta t}{2}[-\frac{F'(\Delta\mathbf{U}_{i,j}^{n}+\tilde{\mathbf{U}}_{i,j})}{\Delta x} + \frac{F'(\tilde{\mathbf{U}}_{i,j})}{\Delta x} - \frac{G'(\Delta\mathbf{U}_{i,j}^{n}+\tilde{\mathbf{U}}_{i,j})}{\Delta y} + \frac{G'(\tilde{\mathbf{U}}_{i,j})}{\Delta y} + S(\Delta\mathbf{U}_{i,j}^{n})]. \tag{42}$$

But since $\Delta\mathbf{U}_{i,j}^{n} = 0$, then we obtain,

$$\Delta\mathbf{U}_{i,j}^{n+\frac{1}{2}} = \frac{\Delta t}{2}\left[-\frac{F'(\tilde{\mathbf{U}}_{i,j})}{\Delta x} + \frac{F'(\tilde{\mathbf{U}}_{i,j})}{\Delta x} - \frac{G'(\tilde{\mathbf{U}_{i,j}})}{\Delta y} + \frac{G'(\tilde{\mathbf{U}}_{i,j})}{\Delta y}\right].$$

Hence, $\Delta\mathbf{U}_{i,j}^{n+\frac{1}{2}} = 0$. Thus we conclude that the updated numerical solution remains stationary up to machine precision.

4. Numerical results

In this section we implement the proposed well-balanced numerical schemes and use them to solve classical problems from the recent literature. The main property of the proposed schemes will be tested when we consider numerical experiments featuring stationary solutions. In our all test cases we will consider an ideal gas with $\gamma = 1.4$ and a parameter value $\theta = 1.5$ for the limiter. The CFL condition is set to 0.485.

4.1. One-dimensional numerical experiments

We start our numerical experiments by verifying that the numerical scheme is capable of preserving any steady state at the discrete level.

4.1.1. One-dimensional isothermal equilibrium

We consider for our first test case the isothermal equilibrium problem with a linear gravitational field $\phi_x = g = 1$ previously considered in [25]. The numerical solution is computed on 200 grid points of the interval [0,1]. The final time is $t = 0.25$. The isothermal equilibrium state is given by:

$$\rho(x) = \rho_0 \exp(-\frac{\rho_0 g}{p_0}x),$$
$$u(x) = 0,$$
$$p(x) = p_0 \exp(-\frac{\rho_0 g}{p_0}x).$$

Here we set $\rho_0 = 1$, $p_0 = 1$. The reference solution $\tilde{\mathbf{u}}$ chosen in this experiment is exactly the isothermal equilibrium state. The results are illustrated in Fig. 1 where we plot the numerical solution at $t = 0.25$ and we compare it to the exact solution. This figure shows that the equilibrium is exactly preserved and a perfect match between the computed solution and the exact one is observed. Note that in [25], this equilibrium needed a very specific well-balanced strategy to be preserved. To test the efficiency of our scheme, a small perturbation is added to the initial pressure. Hence, it is now given as:

$$p(x) = p_0 \exp(-\frac{\rho_0 g}{p_0}x) + \eta \exp(-100\frac{\rho_0 g}{p_0}(x-0.5)^2),$$

where $\eta = 0.01$. In Fig. 2 we plot the perturbation obtained at time $t = 0.25$ and we compare it to the isothermal equilibrium state previously solved on 200 grid points. Outflow boundary conditions are applied. The plots show that the proposed numerical scheme is capable of capturing small perturbation. The order of convergence of the proposed numerical scheme is calculated using the L_1-norm for the density, pressure and the energy components and the obtained results are reported in Table 1.

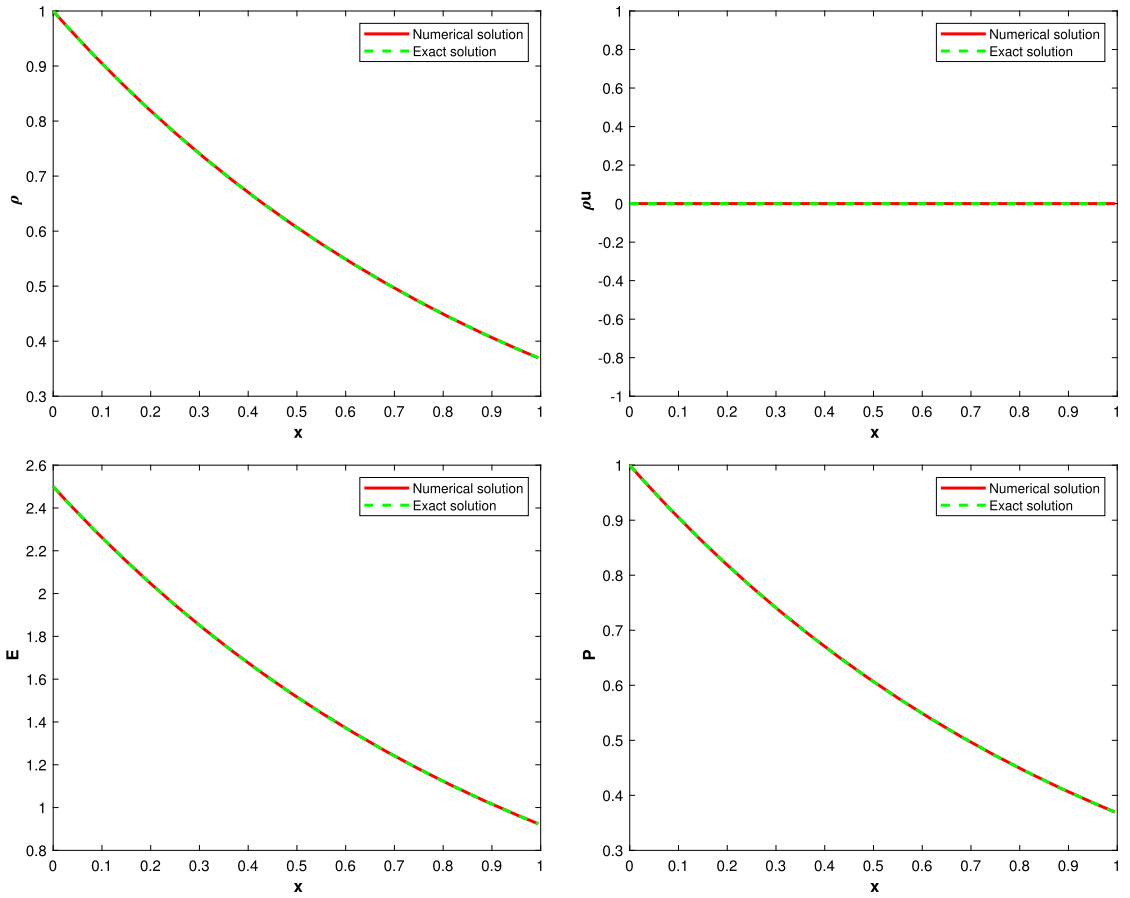

Fig. 1. One-dimensional isothermal equilibrium: Density (top left), momentum (top right), energy (bottom left), pressure (bottom right) at time $t = 0.25$.

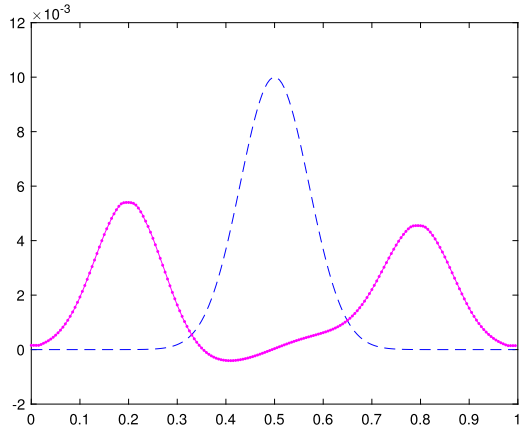

Fig. 2. One-dimensional isothermal equilibrium: Profile of the initial perturbation (dashed curve) and the perturbation at the final time $t = 0.25$ (dotted curve).

Table 1
One-dimensional isothermal equilibrium: L_1-error and order of convergence.

N	L_1-error ρ	Order	L_1-error p	Order	L_1-error E	Order
200	2.7651×10^{-6}	–	3.7978×10^{-6}	–	9.9488×10^{-6}	–
400	7.3147×10^{-7}	1.89	1.0297×10^{-6}	1.88	2.5750×10^{-6}	1.95
800	1.7659×10^{-7}	2.05	2.4007×10^{-7}	2.10	6.0035×10^{-7}	2.19

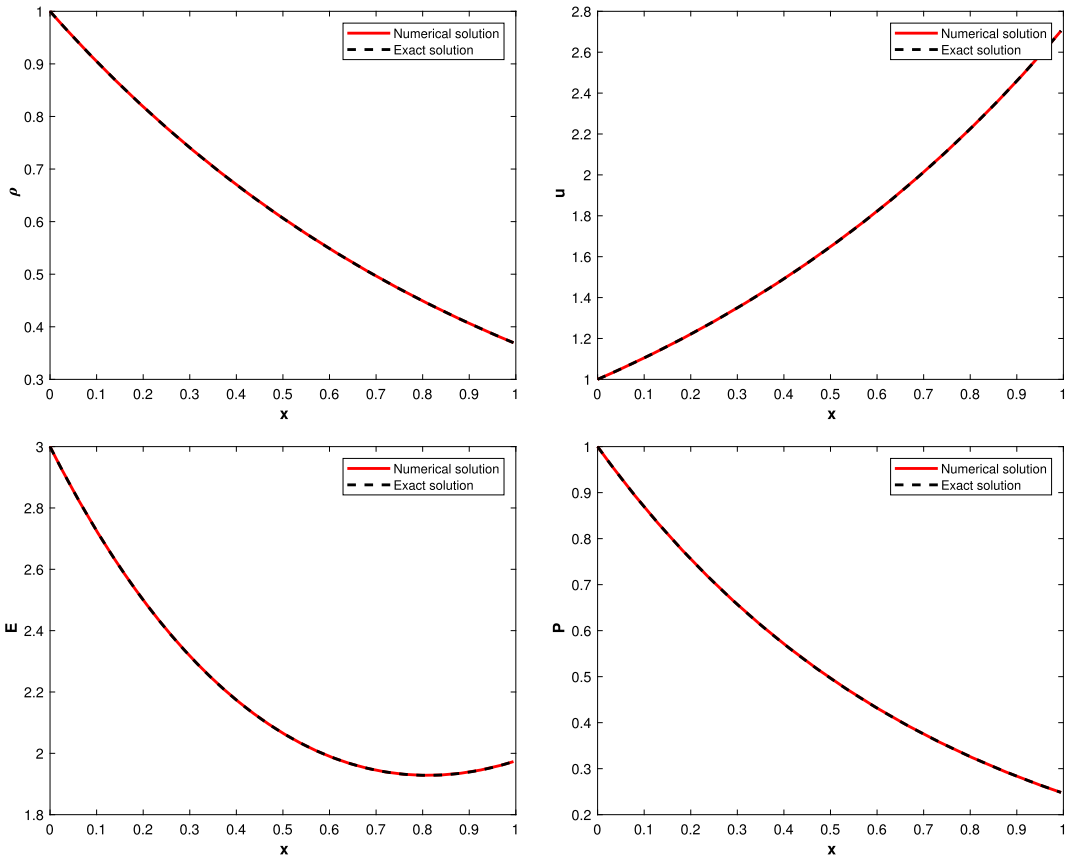

Fig. 3. One-dimensional moving equilibrium: profile of the density (top left), velocity (top right), energy (bottom left), and pressure (bottom right) obtained at time $t = 10$.

4.1.2. One-dimensional moving equilibrium

Next we verify that the proposed numerical scheme is capable of preserving moving equilibrium states. We consider the test case previously presented in [27]. A nonlinear gravitational field $\phi(x) = \exp(x)(-\exp(x) + \gamma(\exp(-\gamma x))$ is considered. The numerical solution is computed at time $t = 10$ on 200 grid points of the interval [0,1]. The moving equilibrium state is given by:

$$\rho(x) = \rho_0 \exp(-\frac{\rho_0 g}{p_0} x),$$
$$u(x) = \exp(x),$$
$$p(x) = \exp(-\frac{\rho_0 g}{p_0} x)^{\gamma}.$$

$\rho_0 = 1$ and $p_0 = 1$ are given. The considered reference solution in this case is the equilibrium state itself. Fig. 3 shows that the density, velocity, energy and pressure are exactly preserved at time $t = 10$. The curves are exactly on top of each other which ensures that the state is perfectly preserved with zero error.

4.1.3. One-dimensional shock tube problem

We consider for our next experiment the shock tube problem with a linear gravitational field with $\phi_x = g = 1$; this problem was previously considered in [25]. The computational domain is the interval [0,1]. Reflecting boundary conditions are considered. The reference solution $\tilde{\mathbf{u}}$ considered in this experiment is the isothermal equilibrium. Notice here that we are not solving steady state problem so any other smooth solution would do the job. The initial conditions are given by:

$$\rho(x) = \begin{cases} 1, & \text{if } x \leq 0.5, \\ 0.125, & \text{otherwise}, \end{cases}$$
$$u(x) = 0,$$

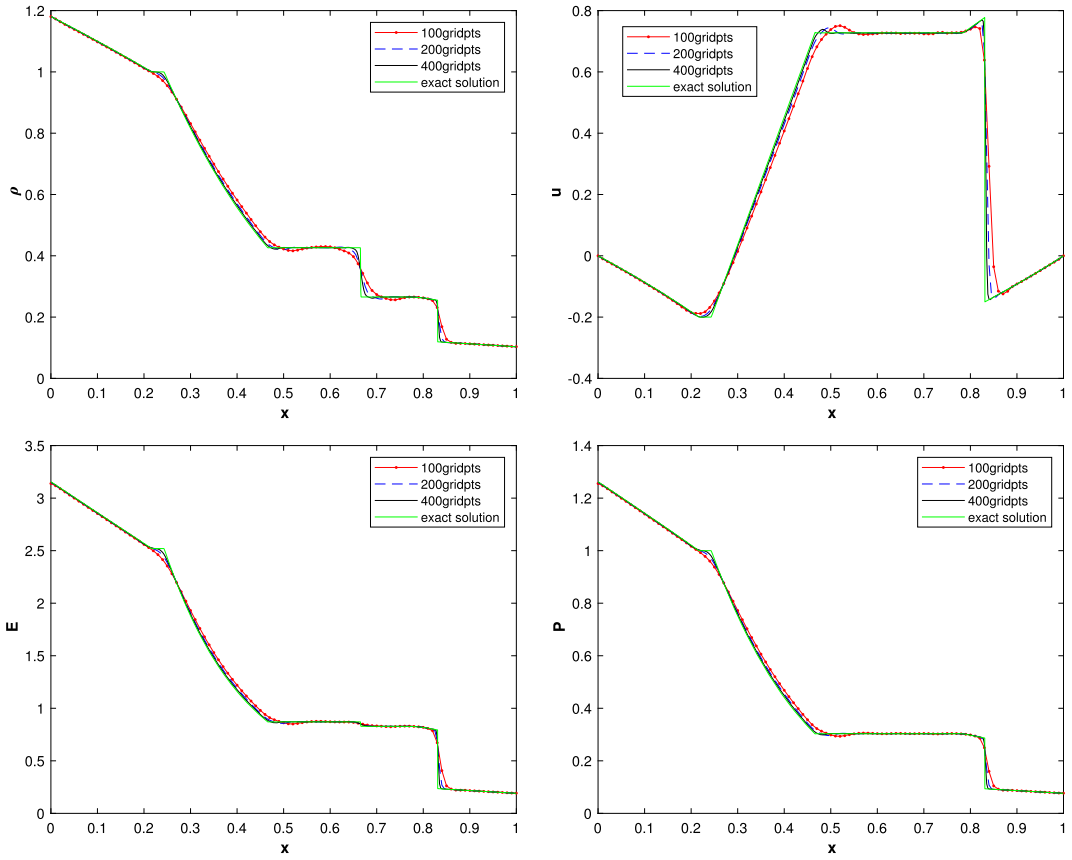

Fig. 4. One-dimensional shock tube problem: Density (top left), velocity (top right), energy (bottom left), pressure (bottom right) at time $t = 0.2$. (For interpretation of the colors in the figure(s), the reader is referred to the web version of this article.)

$$p(x) = \begin{cases} 1, & \text{if } x \leq 0.5, \\ 0.1, & \text{otherwise.} \end{cases}$$

The numerical solution is computed on 100, 200, and 400 grid points at the final time $t = 0.2$. The obtained results are reported in Fig. 4, where we show the profile of the density, velocity, energy, and pressure. The obtained results are in perfect agreement with those appearing in the literature.

4.2. Two-dimensional numerical experiments

In this section we apply the two dimensional well-balanced unstaggered central scheme we developed in section 3 and we solve classical two-dimensional Euler with gravity systems featuring stationary solutions and other equilibrium states.

4.2.1. Two-dimensional isothermal equilibrium

The first numerical experiment we consider is meant to validate the well-balanced property of the proposed two dimensional scheme. We consider the isothermal equilibrium state problem as considered in [6,25,27]. This experiment is a direct extension of the one-dimensional experiment previously considered in subsection 4.1.1. The initial conditions correspond to a stationary state and are given by:

$$\begin{aligned} \rho(x, y) &= \rho_0 \exp(-\frac{\rho_0}{p_0}(g_1 x + g_2 y)), \\ u(x, y) &= 0, \\ v(x, y) &= 0, \\ p(x, y) &= p_0 \exp(-\frac{\rho_0}{p_0}(g_1 x + g_2 y). \end{aligned} \tag{43}$$

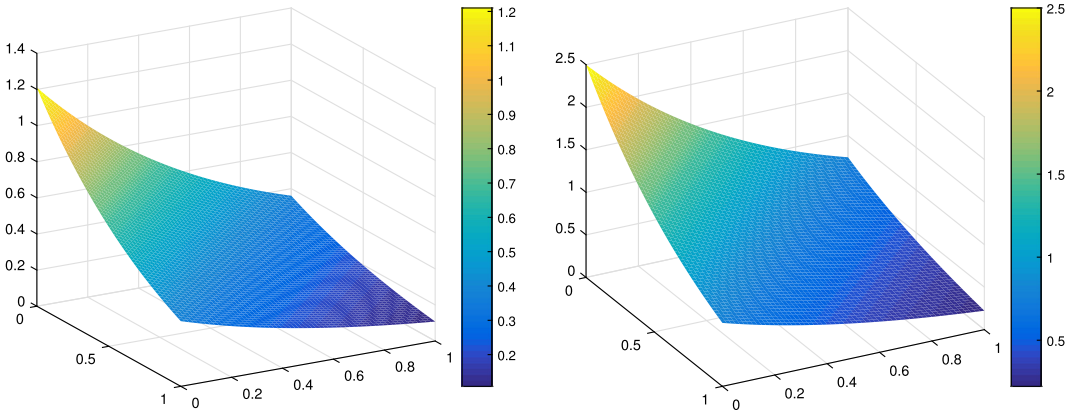

Fig. 5. Two-dimensional isothermal equilibrium: Density (left), energy (right) obtained at the final time $t = 0.25$.

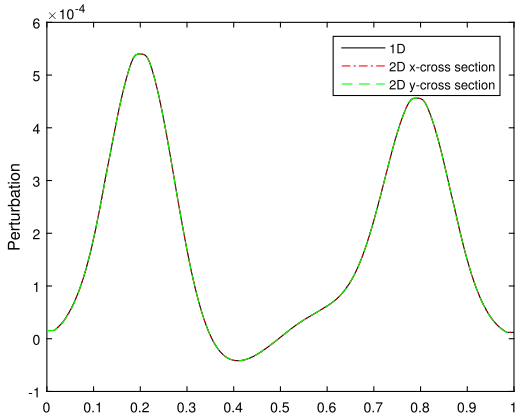

Fig. 6. Unidirectional equilibrium perturbation: 1d/2d comparison of the pressure perturbation at time $t = 0.25$.

$\rho_0 = 1.21$ and $p_0 = 1$ are given. The gravitational potential is linear with $\phi_x = g_1 = 1$ and $\phi_y = g_2 = 1$. The computational domain is the square $[0, 1]^2$ discretized using 60×60 grid points. We apply the two dimensional scheme and compute the numerical solution at the final time $t = 0.25$. Fig. 5 shows the profile of the density and the energy.

4.2.2. Unidirectional equilibrium perturbation

In this test case we extend the one-dimensional perturbation problem to the two-dimensional case where both the equilibrium state and the perturbation are initially set along the $x-$ or y-direction. Whenever set in the $x-$ direction, and similarly to [25], the equilibrium state and the pressure perturbation are given by:

$$\rho(x, y) = \exp(-x)),$$
$$u(x, y) = 0,$$
$$v(x, y) = 0,$$
$$p(x, y) = \exp(-x) + \eta\exp(-100(x - 0.5)^2).$$

Similar initial data is defined if the perturbation is set in the y-direction. The numerical solution is computed at time $t = 0.25$ using our proposed numerical scheme with $\eta = 0.001$; the obtained results are reported in Fig. 7; the observed profiles are similar to those of the one-dimensional case, as well as those reported in the literature. Fig. 6 shows a comparison between cross sections of the pressure of the two-dimensional problem (with perturbations set in the x and y-directions) and the corresponding one of one-dimensional problem; all three curves are in perfect match. The L_1-norm for the density component and the order of convergence of the numerical scheme are reported in Table 2.

4.2.3. Two-dimensional moving equilibrium

This test case is an extension of the one-dimensional moving equilibrium problem to the two-dimensional case; it is meant to verify that the proposed numerical scheme is capable of preserving two-dimensional steady states with non-zero velocities. The initial data is given by:

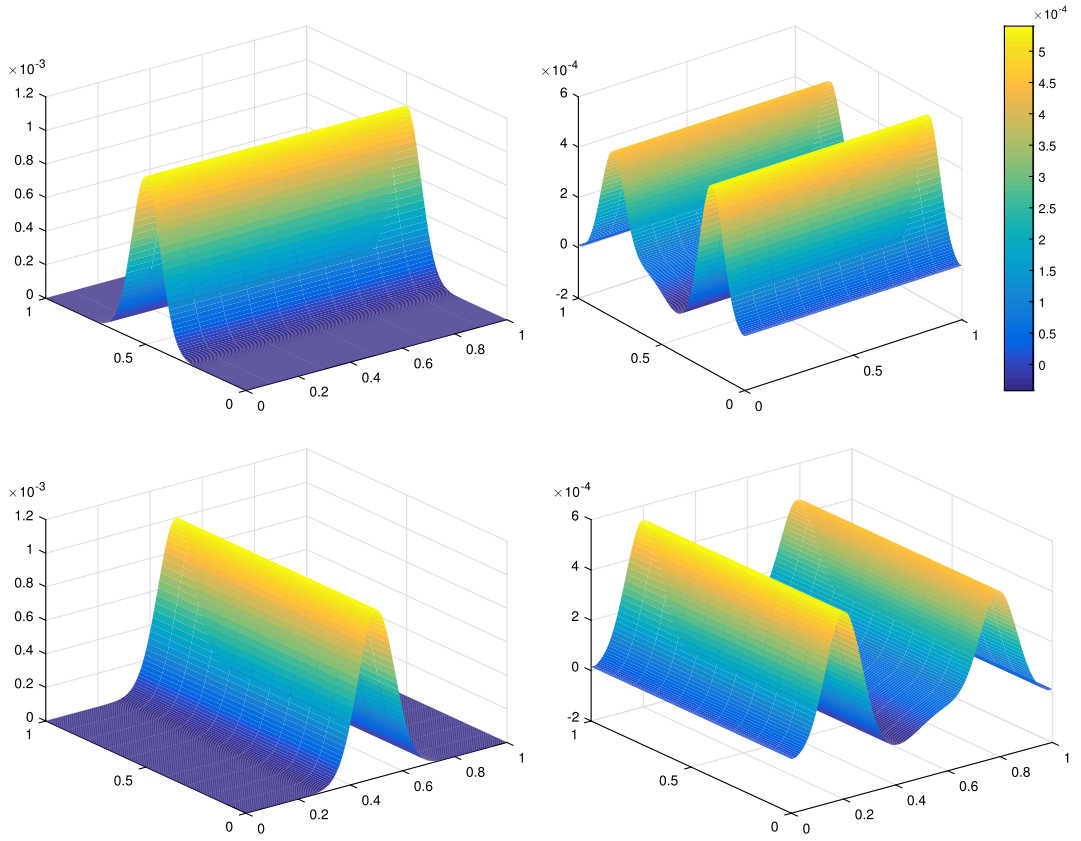

Fig. 7. Unidirectional equilibrium perturbation: Initially along x (top left), at $t = 0.25$ along x (top right), initially along y (bottom left), at $t = 0.25$ along y (bottom right).

Table 2
Unidirectional equilibrium perturbation: L_1-error and order of convergence.

N	L_1-error ρ	Order
200^2	2.8461×10^{-7}	–
400^2	7.0611×10^{-8}	2.01
800^2	1.6840×10^{-8}	2.06

$$\rho(x, y) = \rho_0 \exp(-\frac{\rho_0 g}{p_0}(x + y)),$$
$$u(x, y) = \exp(x + y),$$
$$v(x, y) = \exp(x + y),$$
$$p(x, y) = \exp(-\frac{\rho_0 g}{p_0}(x + y))^{\gamma}.$$

$\rho_0 = 1$, $p_0 = 1$, and $g = 1$. We consider a non-linear gravitational potential given by $\phi(x, y) = \exp(x + y)(-\exp(x + y) + \gamma(\exp(-\gamma(x + y)))$. The numerical solution is computed at the final time $t = 0.25$. The equilibrium is preserved exactly and a 1d/2d comparison is held on the density component at the final time in Fig. 8. The comparison shows a perfect match, thus confirming the potential of the proposed scheme to handle stationary equilibria.

4.2.4. Two-dimensional shock tube problem

We consider for our last experiment the two-dimensional sod shock tube problem. As in the one-dimensional case, the reference solution $\tilde{\mathbf{U}}$ is the isothermal equilibrium solution (43). We consider first the flow along the $x-$ direction with the linear gravitational field with $\phi_x = g_1 = 1$ and $\phi_y = g_2 = 0$; the initial data given by:

$$\rho(x, y) = \begin{cases} 1, & \text{if } x \leq 0.5, \\ 0.125, & \text{otherwise.} \end{cases}$$

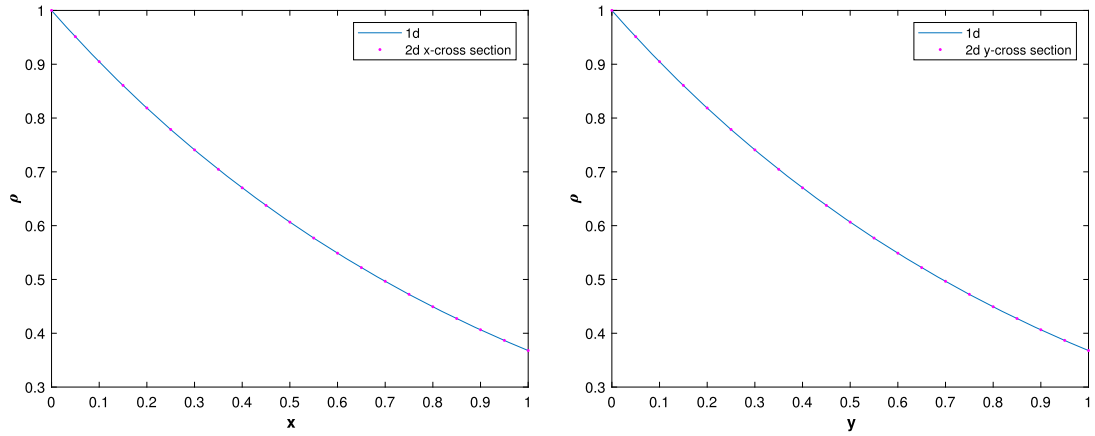

Fig. 8. Two-dimensional moving equilibrium: the density at time $t = 0.25$ with 1d/2d x-cross section (left) and 1d/2d y-cross section (right).

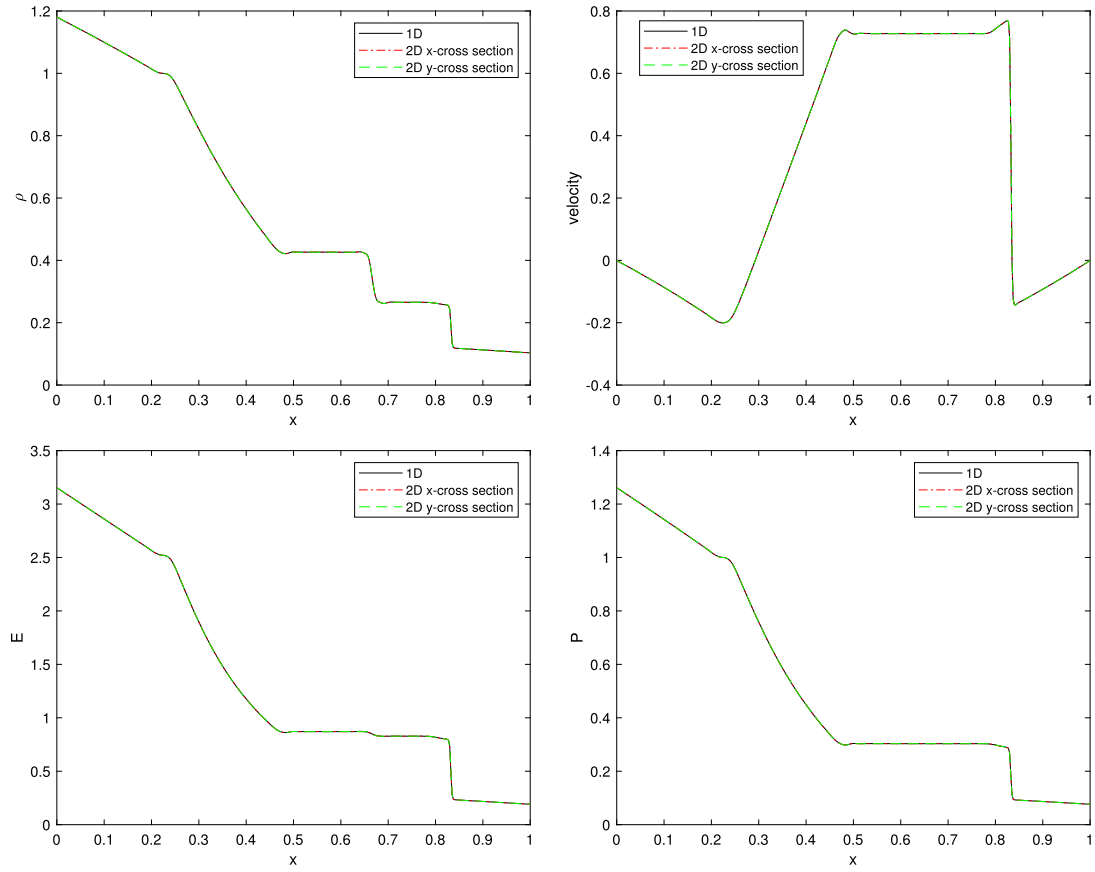

Fig. 9. Two-dimensional shock tube problem: 1d-2d comparison density (top left), velocity (top right), energy (bottom left), pressure (bottom right) at time $t = 0.2$.

$$u(x, y) = 0 = v(x, y).$$

$$p(x, y) = \begin{cases} 1, & \text{if } x \leq 0.5, \\ 0.1, & \text{otherwise.} \end{cases}$$

The computational domain is the square $[0, 1]^2$ discretized using 400×10 grid points. In a similar way we define the initial data along the y-direction, where the same computational domain is discretized using 10×400 grid points. The numerical solution is computed at the final time $t = 0.2$ using the proposed well-balanced scheme and the obtained numerical results are reported. In Fig. 9 we present a comparison between cross sections of the two-dimensional problem

set along the $x-$ and $y-$ directions for the density, velocity, energy and pressure and the corresponding solution of the one-dimensional problem. A perfect match between the plots is observed and the obtained results are in perfect agreement with corresponding ones appearing in the literature.

5. Conclusion

In this work we developed a new second order well-balanced unstaggered central scheme for the system of Euler equations with gravity. The proposed scheme is capable of well-balancing any type of equilibrium states thanks to a special reformulation that computed the numerical solution in terms of a specific reference state. The proposed approach works in both one and two dimensions, and the corresponding numerical schemes are derived. The proposed method is applied in the setup of the Euler with gravity equations but it can be easily extended to other balance laws. The proposed numerical scheme is then tested and classical problems arising in the recent literature were successfully solved. The reported results are in perfect match with their corresponding ones in the literature, thus confirming the potential of the proposed scheme to handle Euler with gravity systems.

Acknowledgements

The first author would like to acknowledge the National Council for Scientific Research of Lebanon (CNRS-L) for granting a doctoral fellowship to Farah Kanbar. The third author would like to acknowledge the Heidelberg Institute for Theoretical Studies grants numbers 822802 and 822860 for their support.

References

[1] P. Arminjon, M.-C. Viallon, Généralization du schéma de Nessyahu-Tadmor pour une équation hyperbolique à deux dimensions d'espace, C. R. Acad. Sci. Paris 320 (1995) 85–88.
[2] P. Arminjon, M.-C. Viallon, Convergence of a finite volume extension of the Nessyahu-Tadmor scheme on unstructured grid for a two-dimensional linear hyperbolic equation, SIAM J. Numer. Anal. 36 (1999) 738–771.
[3] P. Arminjon, M.-C. Viallon, A. Madrane, A finite volume extension of the Lax-Friedrichs and Nessyahu-Tadmor schemes for conservation laws on unstructured grids, Int. J. Comput. Fluid Dyn. 9 (1) (1998) 1–22.
[4] J. Berberich, P. Chandrashekar, C. Klingenberg, High order well-balanced finite volume methods for multi-dimensional systems of hyperbolic balance laws, J. Comput. Phys. (2019).
[5] N. Botta, S. Langenberg, R. Klein, S. Lützenkirchen, Well balanced finite volume methods for nearly hydrostatic flows, J. Comput. Phys. 196 (2004) 539–565.
[6] P. Chandrashekar, M. Zenk, Well-balanced nodal discontinuous Galerkin method for Euler equations with gravity, J. Sci. Comput. (2015), arXiv:1511.08739v1.
[7] A. Chertock, S. Cui, A. Kurganov, S.N. özcan, E. Tadmor, Well-balanced schemes for the Euler equations with gravitation: conservative formulation using global fluxes, arXiv:1712.08218v1, 2017.
[8] I. Christov, B. Popov, New non-oscillatory central schemes on unstructured triangulations for hyperbolic systems of conservation laws, J. Comput. Phys. 227 (11) (2008) 5736–5757.
[9] Vivien Desveaux, Markus Zenk, Christophe Berthon, Christian Klingenberg, A well-balanced scheme for the euler equation with a gravitational potential, in: Finite Volumes for Complex Applications VII-Methods and Theoretical Aspects, Springer, 2014, pp. 217–226.
[10] L. Grosheintz-Laval, R. Käppeli, High-order well-balanced finite volume schemes for the Euler equations with gravitation, J. Comput. Phys. (2019).
[11] A.N. Guarendi, A.J. Chandy, Nonoscillatory central schemes for hyperbolic systems of conservation laws in three-space dimensions, Sci. World J. 2013 (2013).
[12] A. Harten, High resolution schemes for hyperbolic conservation laws, J. Comput. Phys. 49 (1983) 357–393.
[13] G. Jannoun, R. Touma, F. Brock, Convergence of two-dimensional staggered central schemes on unstructured triangular grids, Appl. Numer. Math. 92 (2015) 1–20.
[14] G.S. Jiang, E. Tadmor, Nonoscillatory central schemes for multidimensional hyperbolic conservation laws, SIAM J. Sci. Comput. 19 (6) (1998) 1892–1917.
[15] G.S. Jiang, D. Levy, C.T. Lin, S. Osher, E. Tadmor, High-resolution nonoscillatory central schemes with nonstaggered grids for hyperbolic conservation laws, SIAM J. Numer. Anal. 35 (6) (1998) 2147–2168.
[16] R. Käppeli, S. Mishra, Well-balanced schemes for the Euler equations with gravitation, J. Comput. Phys. 259 (2014) 199–219.
[17] H. Nessyahu, E. Tadmor, Non-oscillatory central differencing for hyperbolic conservation laws, J. Comput. Phys. 87 (2) (1990) 408–463.
[18] G. Puppo, C. Klingenberg, M. Semplice, Arbitrary order finite volume well-balanced schemes for the Euler equations with gravity, J. Sci. Comput. (2019).
[19] R. Touma, Central unstaggered finite volume schemes for hyperbolic systems: applications to unsteady shallow water equations, Appl. Math. Comput. 213 (1) (2009) 47–59.
[20] R. Touma, Unstaggered central schemes with constrained transport treatment for ideal and shallow water magnetohydrodynamics, Appl. Numer. Math. 60 (7) (2010) 752–766.
[21] R. Touma, P. Arminjon, Central finite volume schemes with constrained transport divergence treatment for three-dimensional ideal mhd, J. Comput. Phys. 212 (2) (2006) 617–636.
[22] R. Touma, G. Jannoun, Non-oscillatory central schemes on unstructured grids for two-dimensional hyperbolic conservation laws, Appl. Numer. Math. 62 (8) (2012) 941–955.
[23] R. Touma, S. Khankan, Well-balanced unstaggered central schemes for one and two-dimensional shallow water equation systems, Appl. Math. Comput. 218 (10) (2012) 5948–5960.
[24] R. Touma, C. Klingenberg, Well-balanced central finite volume methods for the ripa system, Appl. Numer. Math. 97 (2015) 42–68.
[25] R. Touma, U. Koley, C. Klingenberg, Well-balanced unstaggered central schemes for the Euler equations with gravitation, SIAM J. Sci. Comput. 38 (5) (2016) 773–807.
[26] D. Varma, P. Chandrashekar, A second-order, discretely well-balanced finite volume scheme for Euler equations with gravity, Comput. Fluids (2019).

[27] M.H. Veiga, D.R. Velasco, R. Abgrall, R. Teyssier, Capturing near-equilibrium solutions: a comparison between high-order discontinuous Galerkin methods and well-balanced schemes, Glob. Sci. (2018), arXiv:1830.5919v2.
[28] Y. Xing, G. Li, Well-balanced discontinuous Galerkin methods for the Euler equations under gravitational fields, J. Sci. Comput. (2016).
[29] Y. Xing, G. Li, Well-balanced discontinuous Galerkin methods with hydrostatic reconstruction for the Euler equations with gravitation, J. Comput. Phys. (2018).
[30] M. Zenk, A. Thomann, C. Klingenberg, A second-order positivity-preserving well-balanced finite volume scheme for Euler equations with gravity for arbitrary hydrostatic equilibria, Int. J. Numer. Methods Fluids 89 (11) (2019).